Journal of Computational Neuroscience 5, 53–69 (1998)

Wave Propagation Mediated by $GABA_B$ Synapse and Rebound Excitation in an Inhibitory Network: A Reduced Model Approach

ZHIXIONG CHEN AND BARD ERMENTROUT
Department of Mathematics, University of Pittsburgh, Pittsburgh, PA 15260
bard@popeye.math.pitt.edu

XIAO-JING WANG
Center for Complex Systems and Department of Physics, Brandeis University, Waltham, MA 02254

Received January 23, 1997; Revised May 13, 1997; Accepted June 4, 1997

Action Editor: John Rinzel

Abstract. A reduction method is used to analyze a spatially structured network model of inhibitory neurons. This network model displays wave propagation of postinhibitory rebound activity, which depends on $GABA_B$ synaptic interactions among the neurons. The reduced model allows explicit solutions for the wavefronts and their velocity as a function of various parameters, such as the synaptic coupling strength. These predictions are shown to agree well with the numerical simulations of the conductance-based biophysical model.

Keywords: sleep spindle rhythm, thalamus, $GABA_B$ receptor, wavefront velocity

1. Introduction

GABA (gamma-aminobutyric acid) is the most prevalent inhibitory neurotransmitter in the central nervous system. There are two main types of GABA receptors, $GABA_A$ and $GABA_B$. The $GABA_A$ receptor is ligand-gated and binds with a Cl^- channel. Its activation produces a brief (about 10 ms) hyperpolarization in the postsynaptic neuron. This rapid synaptic inhibition has been implicated in important functions such as gating signal transmission (Steriade et al., 1990), shaping the response selectivity of cortical neurons (Mize et al., 1992), and synchronizing fast ($\sim$40 Hz) cortical oscillations (Whittington et al., 1995; Wang and Buzsáki, 1996). The action of the $GABA_B$ receptor is slower (100–300 ms), mediated through a G-protein signal pathway, and activates different ion channels at presynaptic and postsynaptic sites. The postsynaptic $GABA_B$ receptor increases a K^+ conductance; while the presynaptic $GABA_B$ receptor reduces the release of neurotransmitter GABA itself, possibly due to the modulation of Ca^{2+} channels. The functional roles of $GABA_B$ synaptic transmission remain not well understood.

Recently, $GABA_B$ synaptic transmission in the thalamus has been a focus of attention in studies of spindle waves that are observed during early stages of quiet sleep (Steriade et al., 1990), as well as *in vitro* in a ferret thalamic slice preparation (von Krosigk et al., 1993; Kim et al., 1995). Detailed network models of thalamic spindle waves have been developed (Wang and Rinzel, 1992, 1993; Wang et al., 1995; Golomb et al. 1994, 1996; Destehxe et al., 1993, 1994, 1996). Golomb et al. (1996) simulated a thalamic model with two neural populations, TC cells (thalamocortical excitatory neurons) and RE cells (reticularis thalami inhibitory neurons), which are reciprocally connected in a spatially structured architecture. In agreement with the ferret slice experiment (Kim et al., 1995), they found that there are complicated waves that move across the network in a "lurching" (that is, discontinuous) manner. Furthermore, the cells left

in the wake of the front do not oscillate synchrously but, instead, break into clusters. However, when the $GABA_A$ receptor is blocked, the efficacy of the $GABA_B$ synaptic inhibition is greatly enhanced and produces a slow, smoothly traveling wave, in the wake of which cells oscillate synchronously. This slow wave propagation phenomenon is the subject of the present study.

In order to carry out a quantitative analysis of the phenomenon, we introduce a minimal version of the thalamic model with only one population of cells. This one-population model may be interpreted as a reduction from a two-population thalamic network to a single population of TC cells. The idea is that, since the TC-to-RE excitation is very rapid (via glutamate receptors of the AMPA type), via the disynaptic TC-RE-TC loop the excitation in a TC cell would result in a barrage of slow $GABA_B$ IPSPs in the neighboring TC cells. This can be mimicked by a single-cell population with $GABA_B$ inhibitory interaction among themselves. In a more general framework, the model presented in this article can be considered as a generic network model of inhibitorily coupled neurons endowed with postinhibitory rebound (PIR) excitation. In Wang and Rinzel (1992, 1993), it has been shown that synchronous ~10 Hz rhythmicity could result from slow mutual inhibition between PIR cells. Here, we show that with a spatially structured network architecture, a population of such neurons coupled by $GABA_B$ synapses, can generate slow-wave propagation similar to the thalamic system with $GABA_A$ receptor blockade.

A key feature of our model is that the synaptic coupling of the cells induces a kind of bistability between the resting state and the oscillatory state. A slow wave can thus be regarded as a wavefront that switches the tissue from rest to rhythmic activity. (Actually, the spindle oscillation waxes and wanes, thus eventually relaxes back to rest; but this occurs at a very slow time scale so we will ignore it.) Model simulations of the RE-TC system attempt to capture the properties of this wavefront, including velocity and the shape of the waves. In this article, we present an analytical study in order to provide a better understanding of the computer simulation results. The slow timescale of $GABA_B$ suggests that one might be able to reduce the biophysical model to a simpler one using the method of averaging. Here, we apply the techniques used in Ermentrout (1994) to reduce the conductance-based network model to a single equation for the $GABA_B$ synapse. This is feasible in the present case, where all the other dynamical variables of the system, including the inactivation of the low-threshold T-type calcium current, are much faster than the $GABA_B$ kinetics. We show that the reduced model we obtain is similar to models that have been analyzed by Ermentrout and McLeod (1993) and by Idiart and Abbott (1993). In these papers, traveling wavefronts are constructed for a bistable scalar equation with coupling via a spatial convolution. We then further approximate the reduced model by a piecewise continuous one, for which we can explicitly determine the shape and velocity of the wavefront.

The article is organized as follows. In Section 2, we describe the conductance-based model and sketch the reduction approach. Section 3 discusses the properties of the reduced model and compares them to the original conductance-based model. We find that the speed curves for the various versions of the reduced model match those computed from the full model. We end with a brief discussion of how the addition of another slow process could lead to a different reduced model and thus to a better description of spindle waves.

2. Biophysical Model and the Reduction

2.1. Description and Simulations

We consider a population of model neurons endowed with a low-threshold calcium current of the T-type, so that these cells show PIR excitation in response to long-lasting synaptic hyperpolarizations (Steriade et al., 1990). The neurons interact with each other via $GABA_B$ inhibitory synapses, as illustrated in Fig. 1. The cells are arranged in a line and coupled via synapses that either decay in strength with distance (exponentially) or are restricted in extent to cells within a fixed distance. Rather than consider the model system as a discrete chain of cells, we look at the continuum analogue. The equations of the network model are

$$\frac{dV}{dt} = -g_T m_\infty^3(V)h(V - V_T) - g_L(V - V_L) - g_{\text{syn}} \int_{-\infty}^{+\infty} \omega(y - y')s^p(y', t)\, dy'(V - V_{\text{syn}}),$$

$$\frac{dh}{dt} = (h_\infty(V) - h)/\tau_\infty(V),$$

$$\frac{dx}{dt} = \alpha_x F(V)(1 - x) - \beta_x x,$$

$$\frac{ds}{dt} = \varepsilon[\alpha_s x(1 - s) - \beta_s s],$$

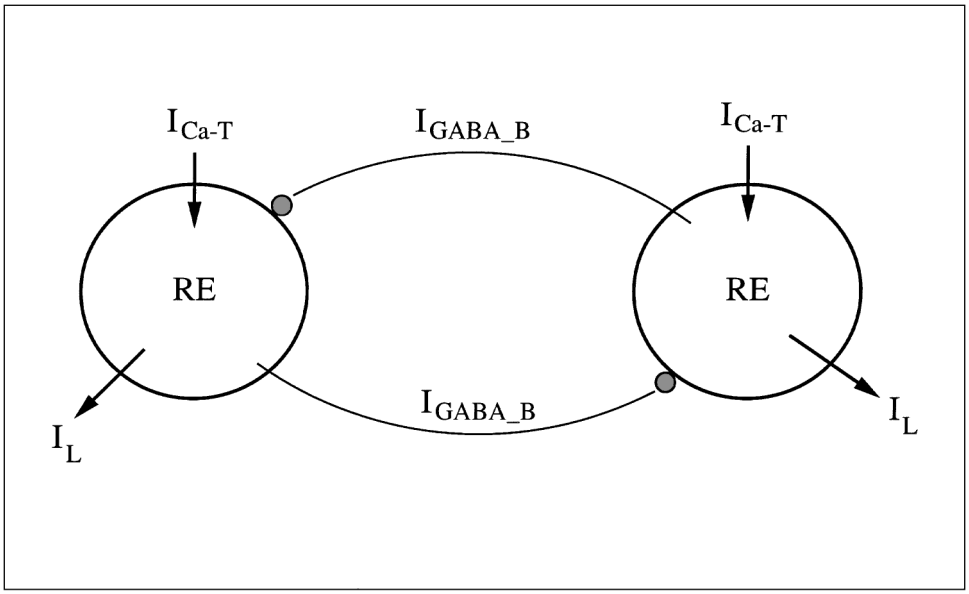

Figure 1. Graphic representation of our inhibition network model, PIR model. All the currents are described in Section 2.1

where the variable y represents the spatial location of the cell. Each neuron has three currents, a leak with conductance g_L, a T-type calcium current with maximal conductance g_T, and the synaptic current with maximal conductance g_{syn}. The activation variable m for the T-type calcium current is assumed to be fast so that it is set at its voltage-dependent steady state $m = m_\infty(V)$. The T-current is responsible for the PIR response, which is a burst of spikes riding on top of the depolarizing wave. In the spirit of a minimal model, however, we did not include spike-generating fast sodium and potassium currents. The effects of an additional slow (for example, calcium-dependent potassium) current will be discussed briefly in the Discussion. The $GABA_B$ synapse is modeled with a two-step kinetics, reflecting the fact that $GABA_B$ inhibition occurs through a G-protein pathway and with a slow onset (Wang et al., 1995). The variable x represents the initial binding and the variable s is the actual synaptic gating variable. The synaptic current is proportional to s^p, with $p = 4$, to take into account the cooperativity of G-proteins in the activation of $GABA_B$ mediated ion channel. The gating variable s changes very slowly as is indicated by the coefficient $\varepsilon \ll 1$. The interaction of the cells is via the spatial summation with weight, $\omega(y)$. This is symmetric and nonnegative and is normalized so that its integral is 1. Golomb et al. (1996) considered two different forms: (1) exponential, $\omega(y) = e^{-|y|/\lambda}/(2\lambda)$ and (ii) step, $\omega(y) = 1/(2\lambda)$ if $|y| < \lambda$ and $\omega(y) = 0$ otherwise. The actual domain of the model is finite over space. However, there can be no constant profile traveling waves over a finite domain (the wave will run off eventually), so we have embedded the network into the whole real line. Thus, a traveling wave can be an asymptotic state. The simulations, of course, are carried out in a discrete and finite space. The details of the functions used in the simulation are given in the Appendix.

Figure 2 shows a typical simulation.The network is initially at rest. A stimulus excites enough cells to produce a wave that travels across the medium at a constant velocity. The front leaves the medium oscillating synchronously in its wake (see Fig. 3). The slope of the excited region in Fig. 2 gives the velocity of the wave. One of the main goals in this article is to determine how the velocity depends on various parameters in the simulation. In particular, we want to understand how the wavefront velocity depends on the synaptic conductance, g_{syn}. Figure 4 shows this dependence for the simulated equations. To calculate the speed accurately, the simulation is run, and the time of the first burst for each cell is recorded. This is then fit to a straight line, and the slope of this line is the reciprocal of the velocity (also see Golomb et al., 1996, p. 758).

2.2. *Fast-Slow Processes*

Since the model has a slow variable s, we will use the reduction approach (Rinzel, 1985; Wang and Rinzel,

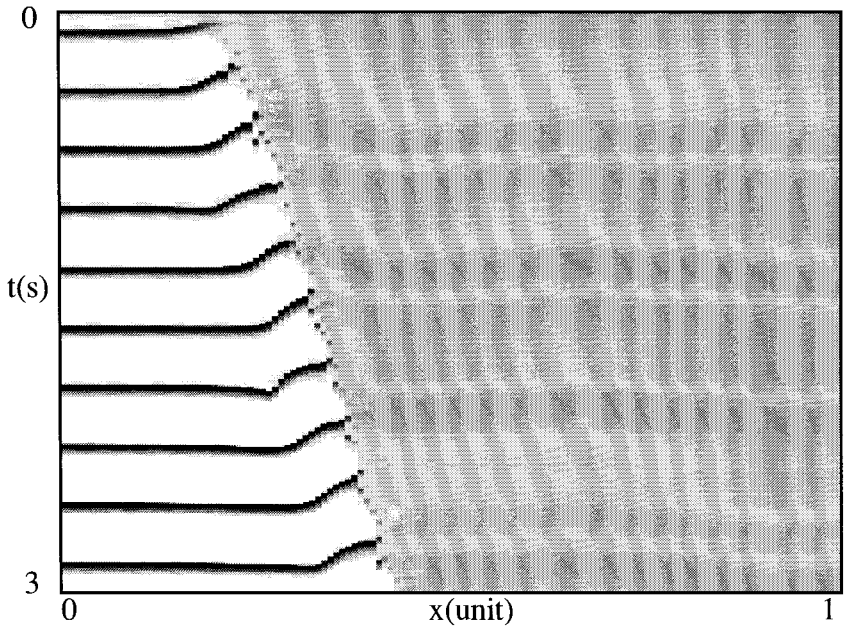

Figure 2. Space-time plot of the voltage for a simulation with parameters as in the appendix. Time increases from top to bottom, and space increases from left to right. Black is 80 mV, and white is −80 mV. Grey is the rest state of about −57 mV. Total length of domain is 1 unit length (say, 1 cm), and the total time of the simulation is 3000 msec.

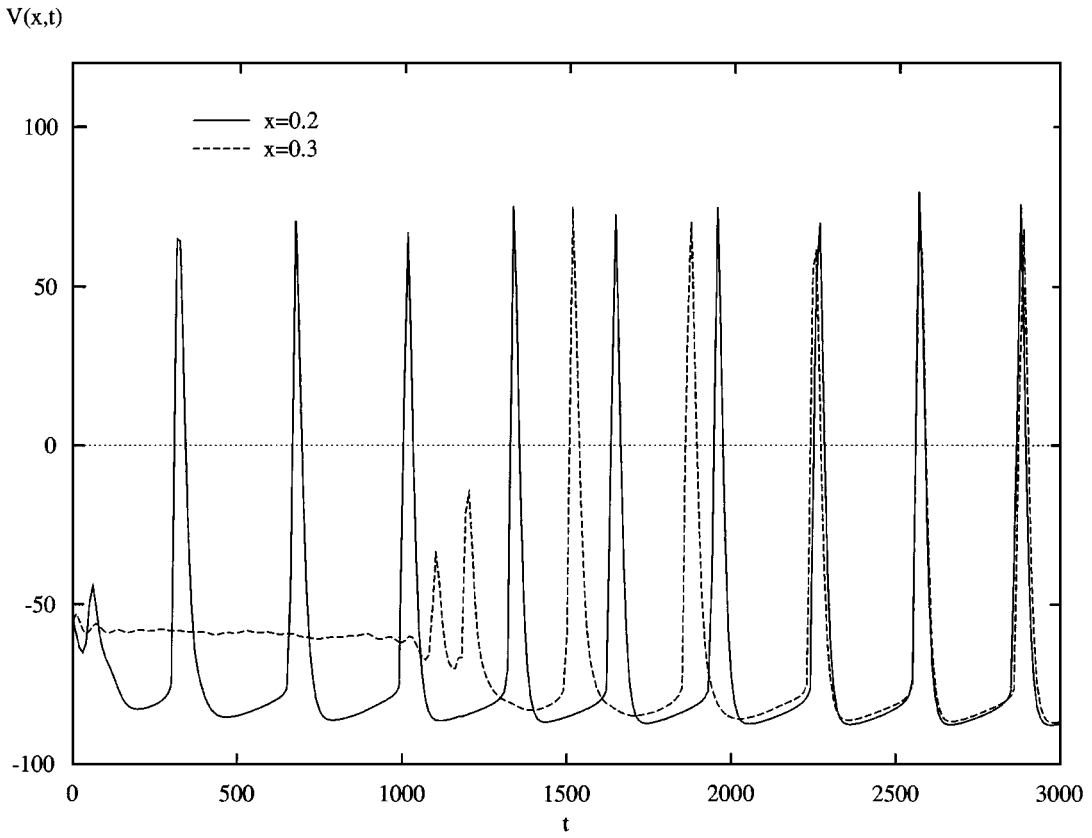

Figure 3. Voltage traces as a function of time at two different spatial points in the simulation of Fig. 2. This shows that synchrony is achieved within a few cycles.

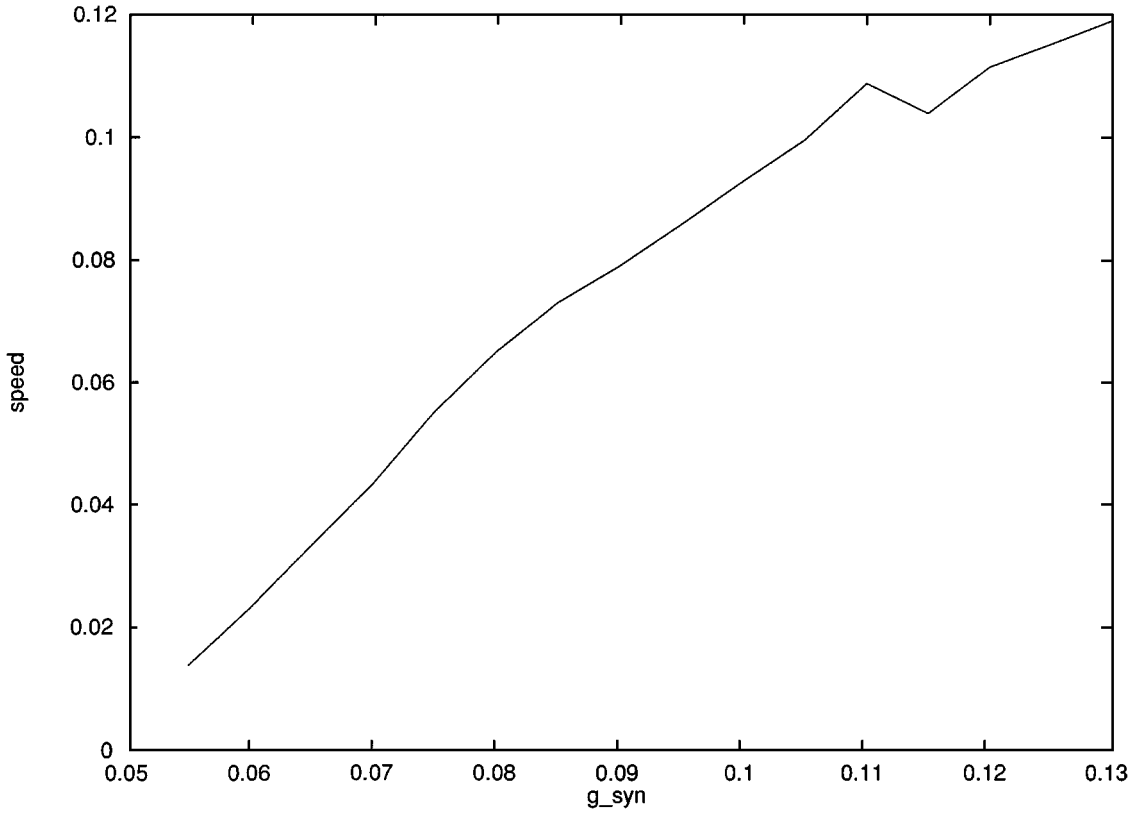

Figure 4. Wavefront velocity of the biophysical model. The velocity is plotted as function of the synaptic conductance, where the x-axis unit is mS/cm^2 and the y-axis is unit-length per second.

1995; Ermentrout, 1994) to simplify the problem. To be specific, consider the following general dynamic system describing an isopotential membrane compartment:

$$\frac{dX}{dt} = F(X, s),$$
$$\frac{ds}{dt} = \varepsilon G(X, s),$$

where $X \in \mathbf{R}^n$ are fast variables and $s \in \mathbf{R}^m$ slow variables. The PIR model is within this framework; V, h, x are fast and s is slow. The basic idea is that since s varies slowly, we first hold s fixed and solve the fast subsystem by treating the slow variables as parameters. Then, in a second step, the dynamical subsystem of the slow variables can be solved in a self-consistent way. For example, suppose that the fast system has $X_0(t; s)$ as a solution with s held fixed. If $X_0(t; s)$ is a steady state—say, $\bar{X}_0(s)$ (that is, it is independent of time)—then we can directly substitute it into the slow system and obtain

$$\frac{ds}{dt} = \varepsilon G(\bar{X}_0(s), s),$$

which is now just a differential equation in s. If, instead, $X_0(t; s)$ is a periodic function of t with period $T(s)$, then we can substitute this into the slow equation and average over the period. The averaged system is then

$$\frac{ds}{dt} = \frac{\varepsilon}{T(s)} \int_0^{T(s)} G(X_0(t; s), s)\, dt,$$

which is also just a differential equation in the slow variables. The Averaging Theorem (Guckenheimer and Holms, 1983) states that this is a reasonable approximation as long as $\varepsilon T(s)$ is sufficiently small. (Strictly speaking these approximations are not valid for slow parameters where the system switches between oscillatory and constant asymptotic behaviors. However, as long as the model is not bistable, this does not present a formal difficulty. To *prove* validity around this point

requires much more work. A recent effort in this direction is given in Soto-Trevino et al., 1996.)

Thus, the averaged equation for the slow subsystem is different depending on whether the fast subsystem behaves as a steady state (fixed point) or an oscillator (limit cycle). We emphasize at this point that we also require that the stable behavior be unique for any given value of the slow parameters s in some range. That is, there *cannot* be, for example, two stable fixed points, or a stable fixed point and a stable limit cycle, for a particular value of s. Having established that, depending on parameters, the fast system either tends to a fixed point or to an oscillation, we must "glue" the two parts together. This requires that we determine the behavior of the fast system as a function of the slow parameters.

We use bifurcation analysis to study the dependence of the fast system on the slow parameters, s. The bifurcation diagram gives us the dependence of the voltage on the parameters, as well as the dependence of the time averages in case the stable behavior is an oscillatory state. Thus, we must solve for the steady state, $X_{\rm ss}$ which satisfies $F(X_{\rm ss}, s) = 0$, and the oscillatory state $X_{\rm oss}(t)$, which satisfies $X'_{\rm oss}(t) = F(X_{\rm oss}(t), s)$. These solutions (or their averages) are substituted into the slow s equations and the resultant slow subsystem is analyzed. We can finally compare the solutions to this reduced system to that of the full system. The reduced system often has the advantage of being either analytically tractable or being much easier to numerically solve.

2.3. *Reduction*

We now return to the PIR model. Rather than treating s as the control or bifurcation parameter in the fast dynamics, we introduce the conductance

$$\bar{g} = g_{\rm syn} \int_{-\infty}^{+\infty} \omega(y - y') s^4(y', t)\, dy' \qquad (1)$$

and use this as the parameter. The fast voltage dynamics satisfies

$$\frac{dV}{dt} = -g_T m_\infty^3(V) h (V - V_T) - g_L (V - V_L) - \bar{g}(V - V_{\rm syn}),$$

and the remaining fast dynamics, h and x, are as above. Thus, for a fixed synaptic conductance $\bar{g}$ we solve the fast system. The only fast variable that appears in the slow synaptic conductance is x, so we need only look at the average of x as a function of $\bar{g}$. Figure 5 shows the average of x along the unique stable solution of the fast dynamics as the synaptic conductance varies. We call this average function

$$G(\bar{g}) = \langle x(t; \bar{g}) \rangle.$$

Note that as the synaptic conductance increases, x actually decreases since the synaptic interaction is inhibitory. However, when hyperpolarized enough, the rest state becomes unstable (due to the deinactivation of the T-type calcium current), and the cell begins to oscillate. The loss of stability is via a Hopf bifurcation, and the resulting small amplitude oscillations are stable for this model. This causes the average of x to grow continuously from the resting value. At higher synaptic inhibition, the oscillation intersects with a fixed point at a saddle-node bifurcation. Only steady-state behavior is possible. In spite of the fact that the system switches from a fixed point to an oscillation and back to a fixed point, the average of the fast variable x remains continuous throughout the parameter range.

From the discussion above, the slow variable satisfies

$$\frac{ds}{dt} = \frac{\varepsilon}{T} \int_0^T (\alpha_s x(t; \bar{g})(1 - s) - \beta_s s)\, dt.$$

But, conveniently enough, the variable over which we are averaging, $x(t)$, appears linearly in the slow equation, so we can rewrite this equation as

$$\frac{ds}{dt} = \varepsilon[\alpha_s G(\bar{g})(1 - s) - \beta_s s].$$

Finally, we can substitute the total synaptic conductance $\bar{g}$ into the slow equation and obtain the reduced equation

$$\frac{ds}{dt} = \varepsilon \left\{ \alpha_s G\left(g_{\rm syn} \int_{-\infty}^{+\infty} \omega(y - y') s^4(y', t)\, dy' \right) \times (1 - s) - \beta_s s \right\}. \qquad (2)$$

The function G was determined numerically; to actually use the slow system of equations, we will approximate the function G by several, increasingly simple, forms. Noting that for low values of $\bar{g}$, G appears to decrease exponentially, we first consider a sum of an exponential and a "bump" function:

$$G(\bar{g}) \approx 0.2 e^{-145\bar{g}} + 0.855 \frac{1}{1 + e^{-2000(\bar{g} - 0.0115)}} \times \frac{1}{1 + e^{900(\bar{g} - 0.0205)}}. \qquad (3)$$

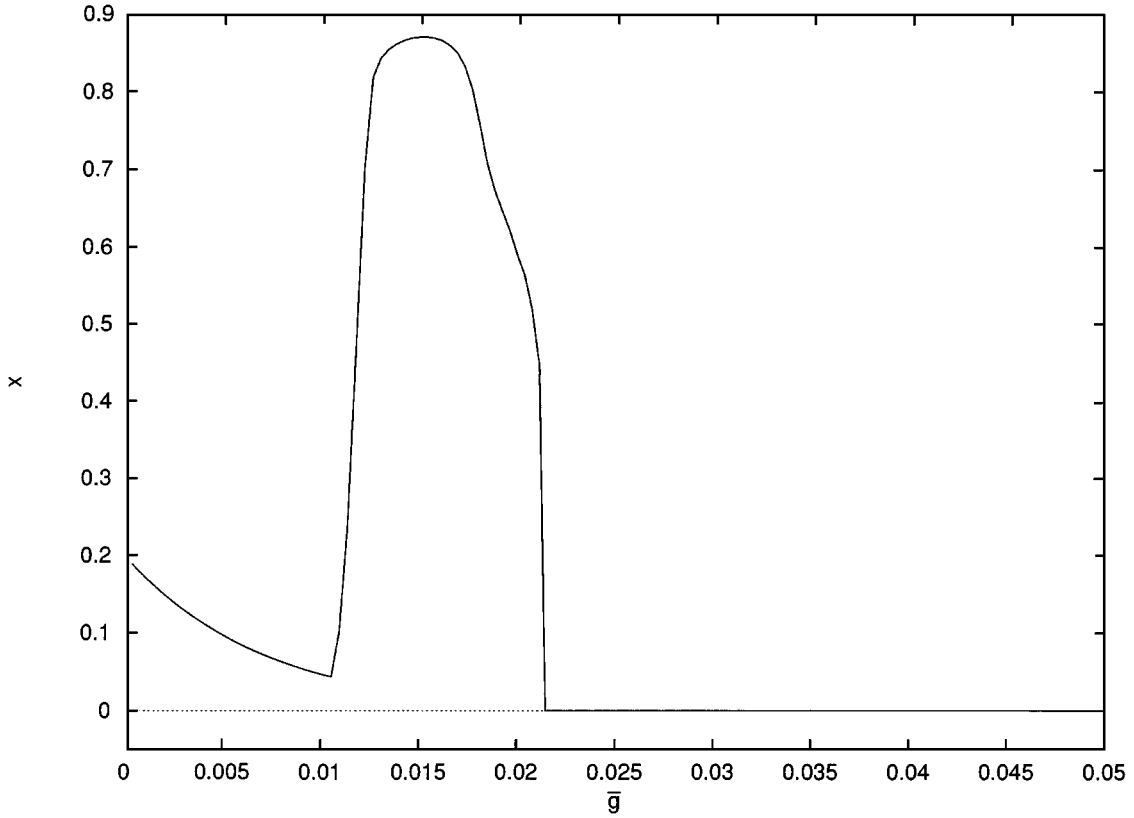

Figure 5. The function G: the average of the fast variable, x as a function of the total synaptic conductance, $\bar{g}$.

This function is shown in Fig. 6 along with the numerically computed version.

Let us make some comments about the reduced model and why one expects to see waves. Consider the "space-clamped" version of Eq. (2):

$$\frac{ds}{dt} = \varepsilon\{\alpha_s G(g_{\text{syn}} s^4)(1-s) - \beta_s s\} \equiv H(s). \quad (4)$$

Under reasonable assumptions on the function G (namely, that it has a "threshold" and rises quickly to some value), the function $H(s)$ has three fixed points, $s_1 < s_2 < s_3$. The lower fixed point is the synaptic activation level when the cell is at rest, and the upper fixed point, s_3, is the synaptic activation level when the cell is firing bursts repetitively. Both of these are stable as solutions to (4). The middle fixed point, s_2, is like a threshold and is unstable. A bistable system with spatial coupling often can give rise to wave fronts that join the two stable fixed points (see, e.g., Ermentrout and McLeod, 1993). That is, there exists a solution to Eq. (2) $s(x,t) = S(x-ct)$ where $S(-\infty) = s_3$ and $S(+\infty) = s_1$. This is a constant profile traveling wave with velocity, c, traveling to the right (if $c > 0$). In front of the wave, the system is at rest and behind, it is in the excited state. Recalling that s is large only when the neuron is bursting repetitively, we see that this wavefront corresponds to a wave that switches the network from rest to repetitively bursting and travels at a constant speed across the tissue. In (Chen et al., 1997) we prove the existence of wavefronts for systems of the form (2) and show that the wavefronts are unique and stable. Thus, for the reduced model, we can understand the basic mechanisms responsible for the propagation of activity across the tissue.

We next compute the speed of the reduced model as a function of g_{syn} by numerically solving the Eq. (2) together with Eq. (3). The velocity is estimated similarly as for the biophysical model. The result of these computations is shown in Fig. 7. The match is very good over the range of parameters used in the full model. (Higher values of g_{syn} result in failure to propagate of any waves; similarly, lower values also cause failure of

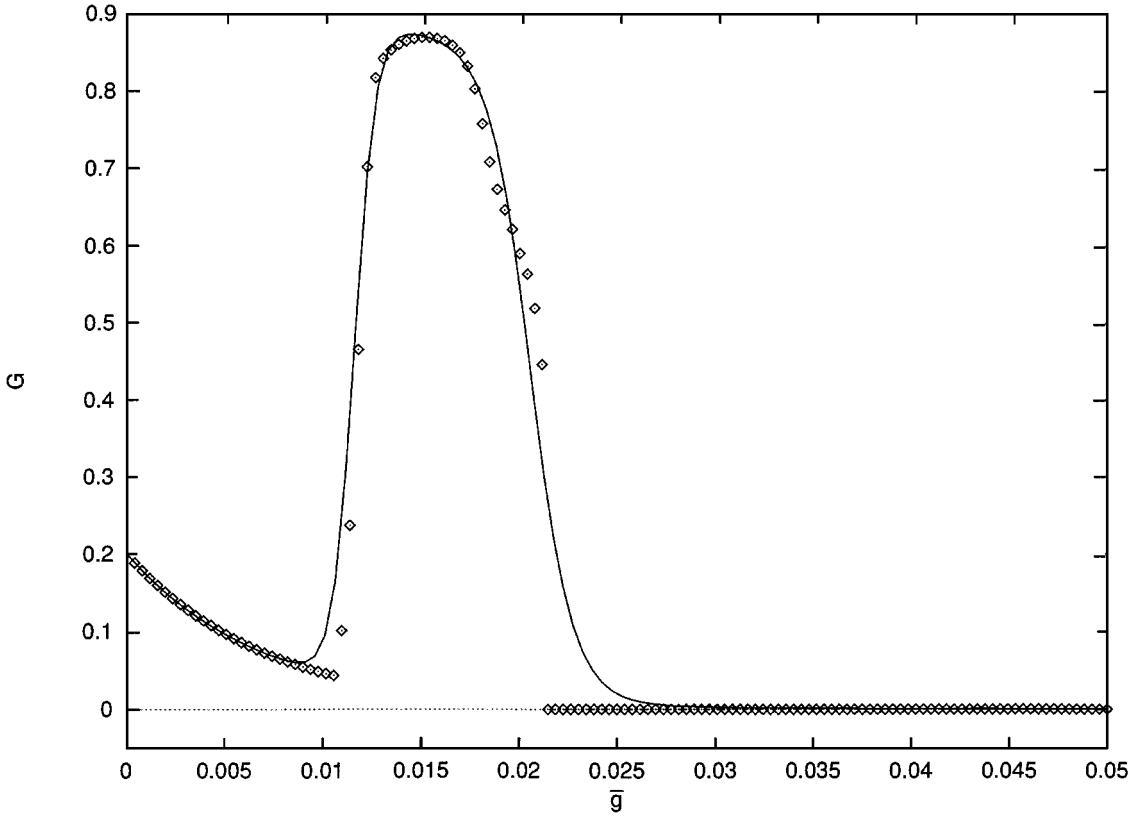

Figure 6. Approximation of the function G (see Eq. (3)).

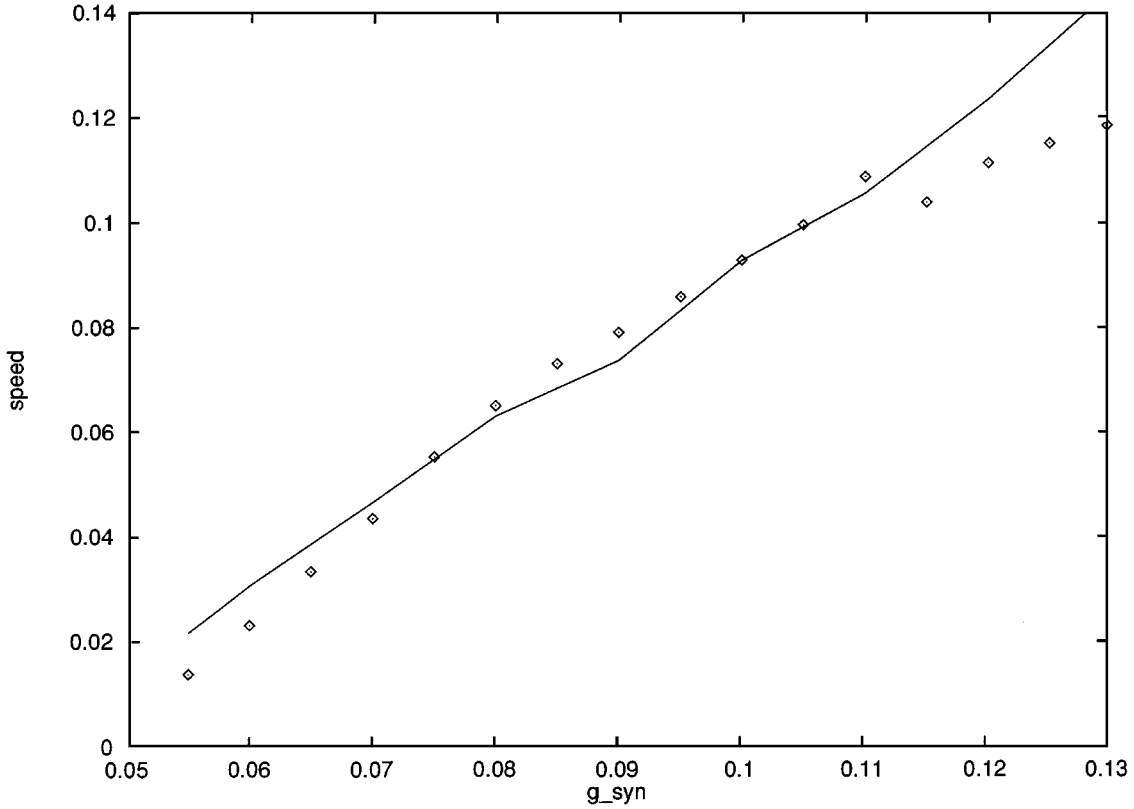

Figure 7. Velocity as a function of the maximal synaptic conductance g_{syn} for the biophysical model. G is defined by Eq. (3). $\omega(\cdot)$ is of exponential type λ, and other parameters are given in the appendix. The dots is the velocity for the PIR model. The unit is same as in Fig. 4.

propagation. This is due to a breakdown of the bistability properties of the reduced model at high values of g_{syn}.)

For the range of g_{syn} values used in the simulations shown in Fig. 7, the total synaptic conductance $\bar{g}$ stays below the value $\simeq 0.015$ corresponding to the maximum of the function G in Fig. 5. This suggests that the part of the function $G(\bar{g})$ for $\bar{g} > 0.015$ is irrelevant for our purposes. Thus, in our next simplification, we approximate the function G by a sigmoid nonlinearity:

$$G(\bar{g}) \approx 0.875/(1 + \exp(-3000(\bar{g} - 0.0115))). \quad (5)$$

We used this expression of $G(\bar{g})$ to numerically simulate the model Eq. (2). The computed wavefront velocity is nearly as good as the one using the more complex form of the function $G(\bar{g})$.

Buoyed by the goodness of the two approximations, we finally turn to the simplest case: approximating $G(\bar{g})$ by a step function. In that case, we can find explicit form solutions to this problem and therefore can calculate the wavefront velocity for all different parameters, as we show in the next section.

3. Wavefronts and Speeds

3.1. Setup for the Analysis

The properties of wavefronts and quantitative information about wavespeed as parameters vary is generally impossible for continuous nonlinearities such as the two approximations described in the previous section. Idiart and Abbott (1993) studied a related problem by linearizing about the threshold and making approximations based on this model. Ermentrout and McLeod (1993) derived expressions for velocity for models similar (but not identical) to Eq. (2) when the nonlinearity is a step-function. Thus, we take G to be the unit step or Heaviside function. Let us define

$$H_r(y) = \frac{M}{1 + \exp\left(-\frac{y}{r}\right)}$$

with $M > 0$. Then Eq. (5) can be written as

$$G_r(\bar{g}) = H_r(\bar{g} - \theta),$$

where θ is a threshold of the sigmoid function H_r, and r is the steepness parameter for sigmoid function. In Eq. (5), ($\theta = 0.0115$ for $r = 1/3000$. Thus, we have the approximate equation for the wavefront:

$$\frac{ds}{dt} = \varepsilon \left\{ \alpha_s H_r \left(g_{\text{syn}} \int_{-\infty}^{+\infty} \omega_\lambda (y - y') s^p(y', t)\, dy' - \theta \right) \times (1 - s) - \beta_s s \right\}, \quad (6)$$

with exponential $\omega_\lambda(y)$.

In Eq. (6), we used the positive number p to replace the exponent 4, since we are interested in the dependence of the network behavior (such as the wavefront velocity) on this exponent.

Let

$$\tau = \beta_s \varepsilon t, \quad \Theta = \frac{\theta}{g_{\text{syn}}}, \quad \sigma = \frac{r}{g_{\text{syn}}}, \quad h = \frac{\alpha_s}{\beta_s} M$$

and define

$$\chi_\sigma(x) = \frac{1}{1 + \exp(-x/\sigma)}.$$

Then Eq. (6) becomes the dimensionless equation,

$$\frac{\partial s}{\partial \tau} = -s + h(1 - s)\chi_\sigma(\omega_\lambda * s^p - \Theta). \quad (7)$$

Here we use the notation for the convolution

$$\omega_\lambda * s^p|_{(y,\tau)} = \int_{-\infty}^{+\infty} \omega_\lambda (y - y') s^p(y', \tau)\, dy'.$$

The sigmoid function $\chi_\sigma(x)$ is almost a step-function, if σ is very small (for example, in Eq. (5), $r = 1/3000$ and if $g_{\text{syn}} = 0.01$, then $\sigma = 0.033$). When $\sigma \to 0^+$, the function $\chi_\sigma(\cdot)$ tends to a Heaviside function—that is,

$$H(x) = \begin{cases} 0, & x < 0 \\ H(0), & x = 0 \\ 1 & x > 0 \end{cases}$$

where $H(0)$ is a value between 0 and 1. By rescaling the space variable, we can assume that the space constant, $\lambda = 1$. Later, we can rescale space to real coordinates whenever needed. Thus, let $\omega = \omega_{\lambda=1}$, we have finally that

$$\frac{\partial s}{\partial \tau} = -s + h(1 - s)H(\omega * s^p - \Theta). \quad (8)$$

In the next subsections, we discuss the wavefront solutions of Eq. (8).

3.2. Traveling Wave Solutions

The space clamped steady-state equation of Eq. (8) is

$$F(s) \equiv -s + h(1-s)H(s^p - \Theta) = 0.$$

If $\Theta \geq 0$, then $s = 0$ is a steady state for any h. Suppose that $0 < \Theta < \kappa^p$. Then $s = \kappa$, where

$$\kappa = \frac{h}{1+h},$$

is another steady state since $H(\kappa^p - \Theta) = 1$ when $\kappa^p - \Theta > 0$. (Note that this follows from our assertion that $H(0)$ lies between 0 and 1; a commonly used value is $H(0) = 0.5$.) There is a "virtual" middle steady state given by $s^p = \Theta$, but due to the discontinuity of the Heaviside step function, this really does not occur (see Fig. 8). As long as $0 < \Theta < \kappa^p$, there are two stable steady states, 0 and κ. The "middle" state, $\Theta^{1/p}$ acts as a separatrix for the two states. If $\Theta > \kappa^p$, then the only steady state is $s = 0$.

We now construct the traveling waves for this simplified model by using a technique similar to that in Ermentrout and McLeod (1993). Our goal is to look for traveling wavefronts that join the two stable states, 0 and κ. We assume that the threshold is in the regime where there are two stable steady states. Therefore, the solution to Eq. (8) is of the form

$$s(y, \tau) = S(\xi),$$

where S is an unknown function of the traveling coordinate, $\xi = y - c\tau$, and c is the velocity of the front. We assume that the excited state is to the left ($S(-\infty) = \kappa$) and the resting state is to the right ($S(+\infty) = 0$). Thus, when the velocity c is positive, the wave switches the system from resting to excitation, and when the velocity is negative, it switches the network from excited to rest. Recall that the excited regime corresponds to repetitive bursting of the voltage. Thus, the fronts we construct here correspond to waves that switch the system from resting potential to rhythmic behavior. By inserting the solution form $s(y, \tau) = S(\xi)$ into Eq. (8), we obtain the traveling wave equation as

$$-cS'(\xi) = -S(\xi) + h(1 - S(\xi))H(\omega * S^p|_\xi - \Theta). \tag{9}$$

We seek monotonic fronts that join the two stable steady states. Thus we assume that S satisfies

$$S(-\infty) = \kappa \quad S(+\infty) = 0.$$

Let us define

$$Z(\xi) \equiv \int_{-\infty}^{+\infty} \omega(\eta) S^p(\xi - \eta)\, d\eta;$$

so

$$H(\omega * S^p|_\xi - \Theta) = H(Z(\xi) - \Theta).$$

Since $\omega(y)$ is positive and has a unit integral and $S \geq 0$, we can find a point ξ_0 such that

$$Z(\xi_0) = \Theta.$$

(To see this, first note that Z is a monotone function of ξ since S is monotone. Then, for a large positive ξ_0 value, S is nearly zero, so the integral is very small. For a very negative ξ_0 value, the integral is close to κ^p which is greater than Θ. Thus there is a unique value of ξ_0.) Since the wave is translation invariant, we can assume that this point, ξ_0, is the origin: $\xi_0 = 0$. This allows us to uniquely determine the wave. Consider $\xi > 0$. Then the integral $Z(\xi)$ is less than Θ, $H(Z(\xi) - \Theta) = 0$, and so Eq. (9) becomes simply

$$-cS' = -S,$$

whose solution in $S^+(\xi) = S_0 e^{\xi/c}$. We want S to tend to 0 as $\xi \to \infty$, so if $c > 0$, we must take $S_0 = 0$, and thus $S(\xi) = 0$ for $\xi > 0$. If $c < 0$ (that is, the wave travels backward turning the medium off), then S_0 is not determined. Now consider $\xi < 0$. Then $Z(\xi) > \Theta$, $H(Z(\xi) - \Theta) = 1$, and Eq. (9) is

$$-cS' = -S + h(1 - S),$$

which has a solution:

$$S^-(\xi) = \kappa + (S_1 - \kappa)e^{\xi(1+h)/c}.$$

Now, if $c < 0$, we must take $S_1 = \kappa$, since we must have that $S(-\infty) = \kappa$. On the other hand, if $c > 0$, then S_1 is arbitrary.

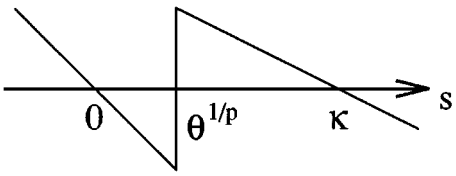

Figure 8. Graph of the steady-state function $F(s)$ showing the two stable steady states 0 and κ separated by the threshold, $s = \Theta^{1/p}$.

We see that there are essentially two cases: $c > 0$ and $c < 0$. Consider $c > 0$ first. We require the solution to be continuous at $\xi = 0$. Thus, $S^-(0) = 0$, which implies that $S_1 = 0$. Thus, if $c > 0$, we have $S(\xi) = 0$ for $\xi > 0$ and $S(\xi) = \kappa(1 - \exp(\xi(1 + h)/c))$ for $\xi < 0$. To determine the velocity, we must use the condition

$$Z(0) = \Theta.$$

By inserting the explicit expression for $S(\xi)$ into this equation, we obtain the following equation for the wavefront velocity:

$$Q_p^+(c) \equiv \kappa^p \int_0^\infty \omega(\eta)(1 - e^{-\eta(1+h)/c})^p \, d\eta = \Theta.$$

It is easy to see that $Q_p^+(0) = \kappa^p/2$ and that $Q_p^+(\infty) = 0$. Furthermore, it is also easy to verify that $Q_p^+(c)$ is a monotonically decreasing function. Thus, as long as Θ lies between 0 and $\kappa^p/2$, there will be a unique positive c such that $Q_p^+(c) = \Theta$. Before explicitly evaluating this integral for specific forms of the weight function ω, we make some observations. For positive velocities—that is, fronts that switch the system from rest to the excited state—we must have that the threshold is less than $\kappa^p/2$. As this critical value is approached, the velocity tends to zero, and we have a "frozen" wavefront that does not travel. Note that this occurs only for a particular value of Θ. A "pathology" of using the Heaviside step function is that as the threshold tends to 0, the velocity tends to infinity. In a smoother approximation, there is a finite maximal velocity found numerically. The velocity increases monotonically as the threshold decreases. The shape of the wavefront sharpens for smaller velocities, and at zero velocity it approaches a step function. The wave is continuous at $\xi = 0$ but not differentiable there. The wavefront is shown in Fig. 9(a) for several different

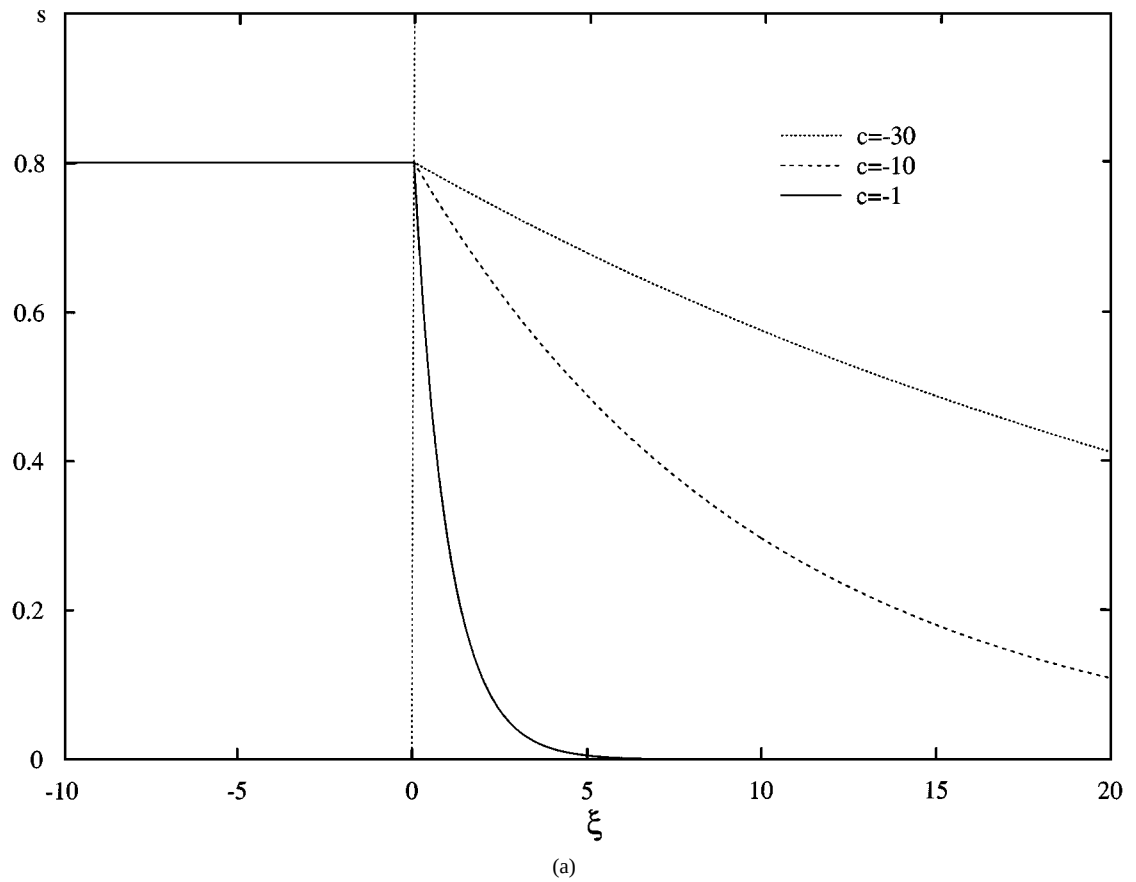

(a)

Figure 9. Exactly determined fronts for the Heaviside nonlinearity case. The synaptic variable s is shown as a function of the traveling coordinate ξ. The speed c shown is a scaled speed. True speed can be obtained by multiplying a constant (see the Appendix). (a) Fronts with different positive velocities; (b) fronts with several negative velocities. (*Continue on next page.*)

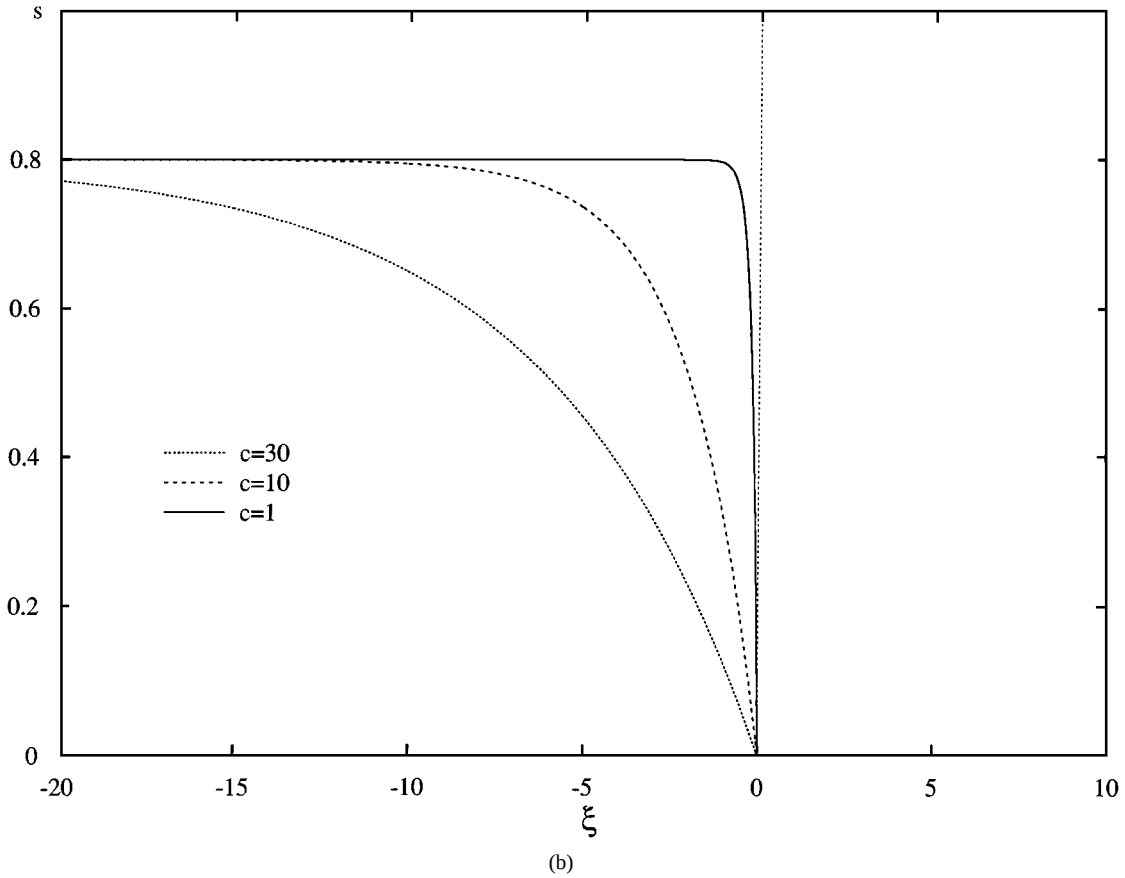

(b)

Figure 9. (*Continued*).

positive velocities and Fig. 9(b) for several different negative velocities.

Now suppose that $c < 0$ (in which case the wavefront moves from the resting state into the oscillatory state and turns off the network activity). Then in analogy to the above discussion, we find that $S_0 = \kappa$, $S(\xi) = \kappa \exp(\xi/c)$ for $\xi > 0$, and $S(\xi) = \kappa$ for $\xi < 0$. The wavefront velocity is given by solving

$$Q_p^-(c) \equiv \kappa^p \left(\frac{1}{2} + \int_0^\infty \omega(\eta) e^{p\eta/c}\, d\eta \right) = \Theta.$$

The function $Q_p^-(c)$ is monotone, $Q_p^-(0) = \kappa^p/2$, and $Q_p^-(-\infty) = \kappa^p$. Thus, in order to have a negative velocity, we need $\kappa^p/2 < \Theta < \kappa^p$. As before, as $\Theta \to \kappa^p/2$, the velocity tends to 0, and we have the frozen wavefront, which is a step function. Similarly, the velocity tends to $-\infty$ as the threshold tends to κ^p. This is a "pathology" of the Heaviside step function. Figure 9(b) shows negative velocity fronts for several different velocities. Note that both positive and negative velocity fronts are constant on one side of the origin and exponential on the other side. Another observation is that the lower is the velocity, the steeper is the front.

3.3. Explicit Calculation of Velocities

To calculate the velocities, we must evaluate the integrals, $Q_p^\pm(c)$ for p and c. MAPLE makes this calculation easy if p is an integer. We can thus express the threshold in terms of the velocity rather than explicitly solving for the velocity:

$$\begin{aligned} \Theta &= Q_p^+(c) \\ &= \frac{\kappa^p}{2} \frac{(1+h)^p p!}{(1+h+c)(2+2h+c)\cdots(p+ph+c)} \end{aligned} \tag{10}$$

$$\Theta = Q_p^-(c) = \frac{\kappa^p}{2} \frac{2c-p}{c-p}. \tag{11}$$

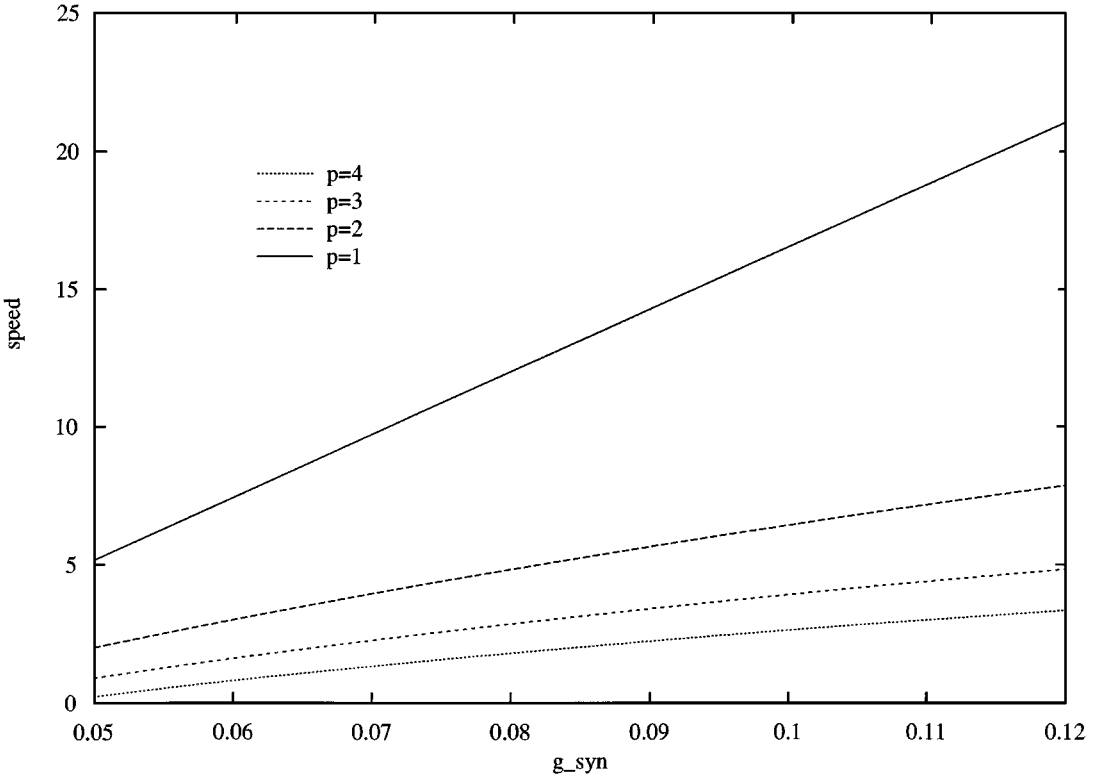

Figure 10. The velocity as a function of the synaptic conductance and the exponent p. (The detailed calculation can be found in the last part of appendix.)

Since $\Theta = \theta/g_{\text{syn}}$ we can now plot the velocity as a function of the maximal synaptic conductance. Recall that we scaled the space constant to be $\lambda = 1$ and scaled the time to be dimensionless (via $\varepsilon\beta_s$). Thus, the velocity in physical unit is given by $c_{\text{true}} = \lambda\varepsilon\beta_s c$, where c is the velocity calculated in the dimensionless equation with $\lambda = 1$. In Fig. 10 we plot the velocity as a function of the synaptic conductance for positive velocities and for $p = 1, 2, 3, 4$ using the values of the parameters κ, θ, and λ given in the Appendix.

Increasing the exponent p reduces the velocity of the waves. For any given synaptic conductance, the choice of p has a drastic effect on the velocity. For example, if $g_{\text{syn}} = 0.08\,\text{mS/cm}^2$, the velocity is about 1.80 (and then 0.0563 unitlength/s) for $p = 4$ and 12.01 (0.375 unitlength/s) for $p = 1$. In Fig. 11, the velocity for the biophysical model and the solvable model are compared.

As a final calculation, we compare the wave-front velocity for several different weight functions, $\omega(y)$: (1) exponential, (2) Gaussian, and (3) the step function:

$$\omega_\lambda(y) = \begin{cases} 0, & |y| > \lambda \\ \frac{1}{2\lambda}, & |y| \le \lambda. \end{cases}$$

The integrals are readily evaluated, the velocity is computed, and the results are plotted in Fig. 12. The velocity is lower by a factor of nearly two for the Gaussian and the step function. The intuition behind this is that the exponential weight function decays much more slowly than the Gaussian or the step function at large distances.

4. Discussion

Nonlinear wave propagation has been observed in several nerve systems, such as in the mammalian retina during the development (Meister et al., 1991), in the disinhibited hippocampal *in vitro* slices (Miles et al., 1988), in the ferret thalamic slices (Kim et al., 1995), and in the olfactory system of the terrestrial mollusk (Delaney et al., 1994). In general, these waves are

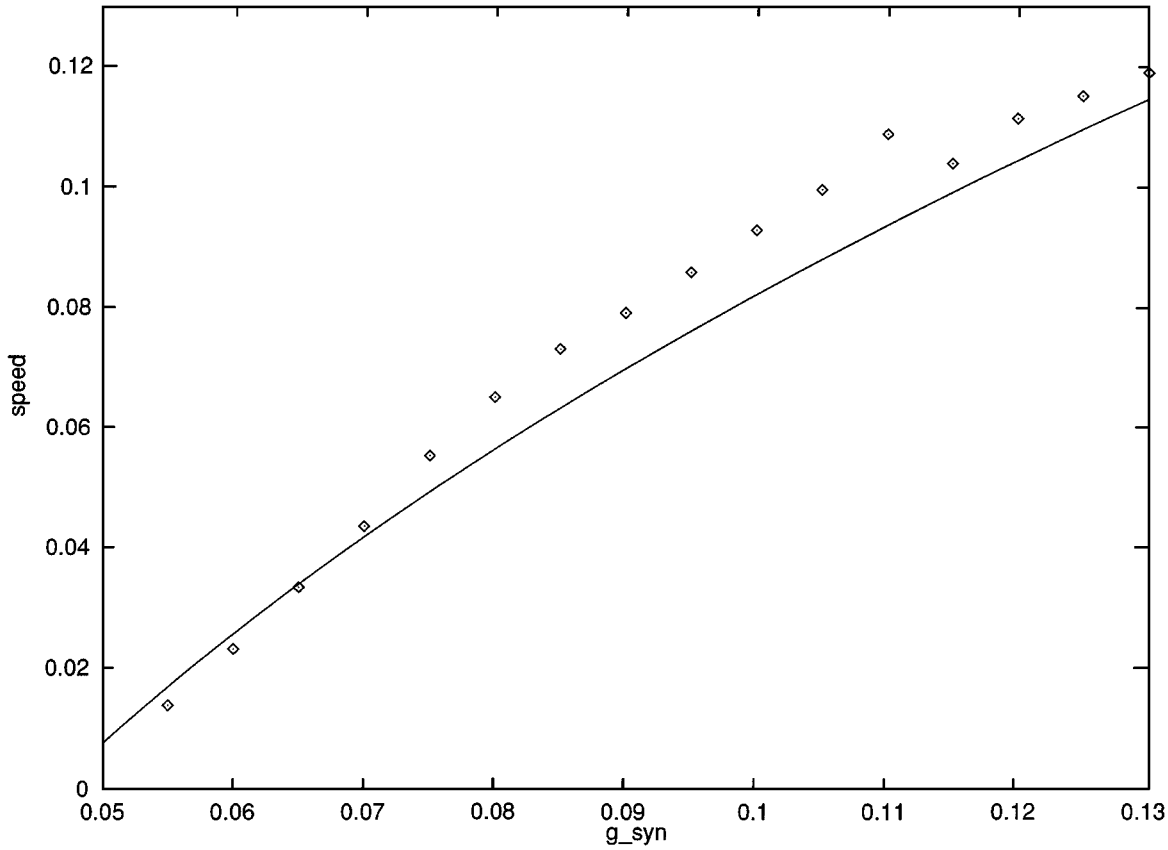

Figure 11. Velocity as a function of the synaptic conductance for $p = 4$ plotted with the velocities computed from the biophysical model.

generated by complex network dynamics involving both synaptic interactions and voltage-dependent intrinsic (ionic) cellular properties. Hence, it is a challenge to develop theoretical tools for quantitatively describing the neuronal wave phenomena, which hopefully can lead to experimentally testable predictions.

In this article, we have focused on a thalamic model of the sleep spindle rhythm and have demonstrated a general approach (the averaging technique) to provide a detailed analysis of the propagating waves. The basic idea is to separate the fast and slow processes and, by averaging over the fast subsystem, reduce the full system to a self-consistent simpler slow subsystem. We have shown how, using this method, one can construct a simple (and in some cases analytically tractable) reduced model in order to understand the propagation of rhythmic activity in the original biophsyical model network. In our case of thalamic spindle oscillation, we have exploited the slow time scale of the inhibitory synapses and averaged over the bursts. The technique is quantitatively accurate in that it fits the simulation results of the full biophysical model very well. There are several computational advantages. First, there are fewer equations to solve. But, more importantly, the simulation can be scaled to the time scale of the slow process since the bursts are averaged out.

One of interesting findings reported here is analytically calculated expressions for the wavefront velocity c as function of the network parameters, such as the connectivity footprint λ and the synaptic coupling strength g_{syn} (see the Appendix). In particular, we found that the velocity c increases with g_{syn} according to a power law,

$$c \simeq g_{\text{syn}}^{1/p},$$

where p is the exponent in the synaptic gating kinetics, $I_{\text{syn}} = g_{\text{syn}} s^p (V - V_{\text{syn}})$ (see Eq. (6)). Such a power-law dependence could have been obtained only with the reduced model, and the prediction compares well with

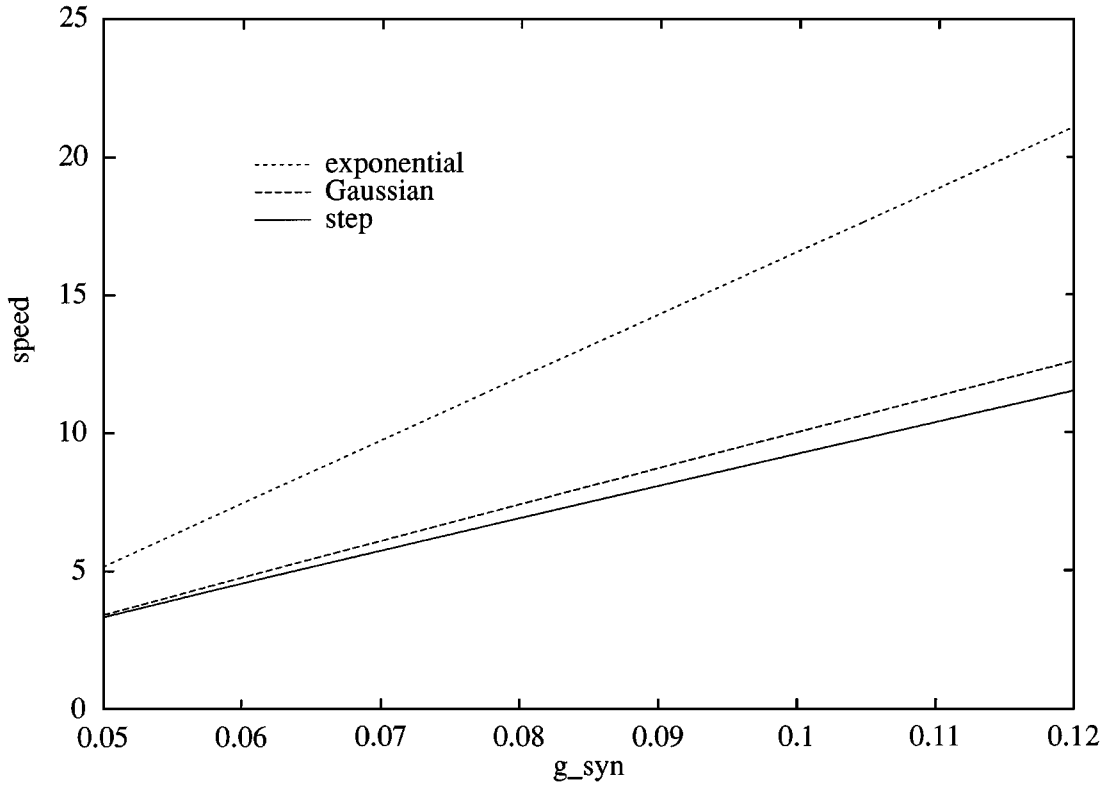

Figure 12. Velocity as a function of the synaptic conductance when $\lambda = 0.0625$ for the exponential weight, the step function weight, and the Gaussian weight. The speeds are scaled. True speed can be obtained by multiplying a constant (see the appendix).

numerical simulations of the original conductance-based model. This example illustrates how such model reduction can yield new results that are capable of predicting the behaviors of the more detailed biophysical network models. Moreover, such a prediction might also be testable experimentally: if a selective $GABA_B$ receptor antigonist could be applied to a ferret thalamic slice that displays spindle waves, with carefully controlled dosages, the spindle wavefront velocity could be measured and plotted versus the drug concentration, and whether the dependence obeys a power law could then be assessed.

In the thalamus, the spindle oscillations wax and wane slowly in time (Steriade et al., 1990; von Krosigk et al., 1993; Kim et al., 1995). In order to account for burst termination as a spindle wanes, other slow processes need to be taken into account (see Destexhe et al., 1996). The analytical framework presented in this article can readily be generalized to include additional slow processes in the model. For example, suppose that some slow conductance, denoted r, acts to terminate the rhythmicity and that r obeys a kinetic equation as

$$\frac{dr}{dt} = \alpha_r(1-r) - \beta_r r,$$

where α_r and β_r depend on fast variables (such as the membrane potential). Then the average synaptic function now also depends on r: $G(\omega * s, r) = \langle x(t; \omega * s, r)\rangle$. Moreover, by averaging over the fast variables, the gating rates for the r-kinetics can be replaced by $A(\omega * s, r) = \langle \alpha_r(t; \omega * s, r)\rangle$, and $B(\omega * s, r) = \langle \beta_r(t; \omega * s, r)\rangle$. Therefore, the reduced synapse model (2) now becomes

$$\frac{ds}{d\tau} = \epsilon\alpha_s G(\omega * s, r)(1-s) - \beta_s s$$
$$\frac{dr}{d\tau} = A(\omega * s, r)(1-r) - B(\omega * s, r)r.$$

This system is similar to the model with slow excitation (by s) and inhibition (by r) that was analyzed in a general context by Ermentrout (1994). A more detailed

description of this type of reduced model is beyond the scope of this article and will be addressed in a later article.

Appendix

Here we present the details of the biophysical network model. In the simulation, we consider the following network:

$$\begin{aligned}
\frac{dV_i}{dt} &= -I_{Ca-T}(V_i, h_i) - I_L(V_i) \\
&\quad - I^{\mathrm{RR}}_{\mathrm{GABA}_B}\big(V_i, \{s_{B_j}\}\big), \\
\frac{dh_i}{dt} &= (h_\infty(V_i) - h_i)/\tau_h(V_i), \\
\frac{dx_{B_j}}{dt} &= \alpha_x F(V_j)(1 - x_{B_j}) - \beta_x x_{B_j}, \\
\frac{ds_{B_j}}{dt} &= \varepsilon\big[\alpha_s x_j\big(1 - s_{B_j}\big) - \beta_s s_{B_j}\big].
\end{aligned}$$

where

$$\begin{aligned}
I_{Ca-T}(V, h) &= -g_{Ca} m^3_\infty(V) h (V - V_{Ca}) \\
I_L(V) &= -g_L(V - V_L) \\
I^{\mathrm{RR}}_{\mathrm{GABA}_B}\big(V_i, \{s_{B_j}\}\big) &= -g_{\mathrm{syn}}(V_i - V_{\mathrm{syn}}) \\
&\quad \times \sum_{j=1}^{N} \omega_{\mathrm{RR}}(i - j) s^4_{B_j}.
\end{aligned}$$

and

$$\begin{aligned}
m_\infty(x) &= \frac{1}{1 + \exp\big(-\frac{x+65}{7.8}\big)}, \\
h_\infty(x) &= \frac{1}{1 + \exp\big(\frac{x+79}{5}\big)}, \\
\tau_h(x) &= \frac{1}{2}\left\{20 + h_\infty(x)\exp\left(\frac{x + 162.3}{17.8}\right)\right\}.
\end{aligned}$$

All other parameters are as follows:

$$\begin{aligned}
g_{Ca} &= 1.0\ \mathrm{mS/cm^2}, \quad g_L = 0.04\ \mathrm{mS/cm^2}, \\
g_{\mathrm{syn}} &= 0.1\ \mathrm{mS/cm^2}. \\
V_{Ca} &= 120.0\ \mathrm{mV}, \quad V_L = -75\ \mathrm{mV}, \\
V_{\mathrm{syn}} &= -100\ \mathrm{mV}, \\
\alpha_x &= 5.0\ \mathrm{ms^{-1}}, \quad \beta_x = 0.007\ \mathrm{ms^{-1}}, \\
\varepsilon\alpha_s &= 0.03\ \mathrm{ms^{-1}}, \quad \varepsilon\beta_s = 0.005\ \mathrm{ms^{-1}},
\end{aligned}$$

and

$$\begin{aligned}
F(V) &= \frac{1}{1 + \exp\big(-\frac{x+40}{2.0}\big)}, \\
\omega_{\mathrm{RR}}(i - j) &= \frac{1}{2\lambda}\exp\left(-\frac{|i - j|}{\lambda}\right).
\end{aligned}$$

In the simulation, we take $N = 128$ cells, and the footprint is $\lambda = 8$ cells. Initially, 16 cells are hyperpolarized to the rebound level. The corresponding parameters in the reduced model are as follows: $\varepsilon = 0.01$, and $M = 0.875$, which is the maximum height of the function G (see Fig. 6). Therefore,

$$h = 5.25, \qquad \kappa = 0.84, \qquad \tau = 0.005t.$$

We find $\theta = 0.0115$, so $\Theta = 0.0115/g_{\mathrm{syn}}$. Moreover, $\lambda = 8/128 = 0.0625$.

Finally, we can easily find velocities for $p = 1$, 2, 3, 4 from Eq. (10) and Eq. (11). For example, we find for $p = 1$ that

$$c = -(1 + h)\frac{2\Theta - \kappa}{2\Theta} = -6.25 + 228.26 g_{\mathrm{syn}}.$$

Back to the physical unit, since we have scaled the space and time, the speeds drawn are $\lambda\beta_s c$. Notice our time unit is second. Similarly, we see that for $p = 2, 3, 4$, respectively,

$$\begin{aligned}
c &= -(1 + h)\left\{\frac{3}{2} - \sqrt{\frac{1}{4} + \frac{\kappa^2}{\Theta}}\right\} \\
&= -9.375 + 6.25\sqrt{(0.25 + 61.356 g_{\mathrm{syn}})}, \\
c &= -(1 + h)\left\{2 - \left[\frac{3\kappa^3}{2\Theta} - \sqrt{-\frac{1}{27} + \frac{9\kappa^6}{4\Theta^2}}\right]^{\frac{1}{3}}\right. \\
&\qquad \left. - \left[\frac{3\kappa^3}{2\Theta} + \sqrt{-\frac{1}{27} + \frac{9\kappa^6}{4\Theta^2}}\right]^{\frac{1}{3}}\right\} \\
&= -12.5 + 6.25\Big(77.30 g_{\mathrm{syn}} \\
&\qquad - \sqrt{0.037 + 5973.9 g^2_{\mathrm{syn}}}\Big)^{0.333} \\
&\quad + 6.25\Big(77.30 g_{\mathrm{syn}} + \sqrt{-0.037 + 5973.9 g^2_{\mathrm{syn}}}\Big)^{0.333}
\end{aligned}$$

and

$$\begin{aligned}
c &= -(1 + h)\left\{\frac{5}{2} - \sqrt{\frac{5}{4} + \sqrt{1 + \frac{12\kappa^4}{\Theta}}}\right\} \\
&= -15.625 + 6.25\sqrt{1.25 + \sqrt{1 + 519.5 g_{\mathrm{syn}}}}.
\end{aligned}$$

Finally, the negative speed is given uniformally by

$$c = \frac{p}{2}\frac{\kappa^p - 2\Theta}{\kappa^p - \Theta}, \qquad \forall p.$$

Acknowledgments

The work was partly supported by NSF and NIMH (to GBE); by the NSF (IBN-9409202), the NIMH (MH53717) and the Alfred P. Sloan Foundation (to XJW).

References

Bates P, Fife P, Ren X, Wang X (1996) Travelling waves in a convolution model for phase transitions. *Arch Rat Mech Ana*.

Chen Z, Ermentrout B, McLeod B (1997) Travelling fronts for a class of non-local convolution differential equations. *Applicable Analysis*, 64:235–253.

Delaney K.R, Gelperin A, Fee MS, Flores JA, Gervais R, Tank DW, Kleinfeld D (1994) Waves and stimulus-modulated dynamics in an oscillating olfactory network. *Proc. Natl. Acad. Sci. (USA)* 91:669–673.

Destexhe A, McCormick DA, Sejnowski TJ (1993) A model for 8–10 Hz spindling in interconnected thalamic relay and reticularis neurons. *Biophys. J.* 65:2473–2477.

Destexhe A, Contreras D, Sejnouski TJ, Steriade M (1994) A model of spindle rhythmicity in the isolated thalamic reticular nucleus. *J. Neurophysiol.* 72:803–818.

Destexhe A, Bal T, McCormick DA, Sejnouski TJ (1996) Ionic mechanisms underlying synchronized oscillations and propagating waves in a model of ferret thalamic slices. *J. Neurophysiol*. 76:2049–2070.

Ermentrout GB (1994) Reduction of conductance based models to neural nets. *Neural Computation* 6:679–695.

Ermentrout B, McLeod J (1993) Existence and uniqueness of travelling waves for a neural network. *Proceedings of the Royal Society of Edinburgh* 123A:461–478.

Golomb D, Wang X-J, Rinzel J (1994) Synchronization properties of spindle oscillations in a thalamic reticular nucleus model. *J. Neurophysiol*. 72:1109–1126.

Golomb D, Wang X-J, Rinzel J (1996) Propagation of spindle waves in a thalamic slice model. *J. Neurophysiol*. 75:750–769.

Guckenheimer J, Holms P (1993) Nonlinear Oscillations, Dynamical Systems and Bifurcations of Vector Field. Springer-Verlag, New York.

Idiart MAP, Abbott L (1993) Propagation of excitation in neural-network models. *Network* 4:285–294.

Kim U, Bal T, McCormick DA (1995) Spindle waves are propagating synchronized oscillations in the ferret LGNd in vitro. *J. Neurophysiol.* 74:1301–1323.

Meister M, Wong ROL, Baylor DA, Chatz CJ (1991) Synchronous bursts of action potentials in ganglion cells of the developing mammalian retina. *Science* 252:939–943.

Miles R, Traub RD, Wong KS (1988) Spread of synchronous firing in longitudinal slices from the CA3 region of the hippocampus. *J. Neurophysiol*. 60:1481–1496.

Mize RR, Marc RE, Sillito AM, eds. (1992) GABA in the retina and central visual system. *Progress in Brain Research*, vol. 90. Elsevier, Amsterdam.

Orlandi E, Triolo L (1995) Travelling fronts in non-local models for phase separation in external field. *CARR Reports in Mathematical Physics*, June.

Rinzel J (1985) Bursting oscillations in an excitable membrane model. In Ordinary and Partial Differential Equations. *Proceedings of the Eighth Dundee Conference* 304–316.

Soto-Trevino C, Kopell N, Watson D (1996) Parabolic bursting revisited. *J. Math. Biology* 35:114–128.

Steriade M, Jones EG, Llinás RR (1990) Thalamic Oscillations and Signaling. New York, Wiley.

von Krosigk M, Bal T, McCormick DA (1993) Cellular mechanisms of a synchronized oscillation in the thalamus. *Science* 261:361–364.

Wang X-J, Rinzel J (1992) Alternating and synchronous rhythms in reciprocally inhibition model neurons. *Neural Computation* 4:84–97.

Wang X-J, Rinzel J (1993) Spindle rhythmocity in the reticularis thalami nucleus-synchronization among inhibitory neurons. *Neurosci*. 53:899–904.

Wang X-J, Rinzel J (1995) Oscillatory and bursting properties of neurons. In: M. Arbib, ed., Handbook of Neural Networks and Brain Theory. MIT Press, Cambridge, MA. pp. 686–691.

Wang X-J, Golomb D, Rinzel J (1995) Emergent spindle oscillations and intermittent burst firing in a thalamic model: Specific neuronal mechanisms. *Proc. Natl. Acad. Sci. (USA)* 92:5577–5581.

Wang X-J, Buzsáki G (1996) Gamma oscillation by synaptic inhibition in a hippocampal interneuronal network model. *J. Neurosci*. 16:6402–6413.

Whittington MA, Traub RD, Jeffreys JGR (1995) Synchronized oscillations in interneuron networks driven by metabotropic glutamate receptor activation. *Nature* 373:612–615.